SAR Image Denoising via Bayesian Wavelet Shrinkage Based on Heavy-Tailed Modeling

Alin Achim, *Student Member, IEEE*, Panagiotis Tsakalides, *Member, IEEE*, and Anastasios Bezerianos, *Member, IEEE*

***Abstract*—Synthetic aperture radar (SAR) images are inherently affected by multiplicative speckle noise, which is due to the coherent nature of the scattering phenomenon. This paper proposes a novel Bayesian-based algorithm within the framework of wavelet analysis, which reduces speckle in SAR images while preserving the structural features and textural information of the scene. First, we show that the subband decompositions of logarithmically transformed SAR images are accurately modeled by alpha-stable distributions, a family of heavy-tailed densities. Consequently, we exploit this a priori information by designing a maximum *a posteriori* (MAP) estimator. We use the alpha-stable model to develop a blind speckle-suppression processor that performs a nonlinear operation on the data and we relate this nonlinearity to the degree of non-Gaussianity of the data. Finally, we compare our proposed method to current state-of-the-art soft thresholding techniques applied on real SAR imagery and we quantify the achieved performance improvement.**

***Index Terms*—Maximum *a posteriori* (MAP) estimation, symmetric alpha-stable distributions, synthetic aperture radar (SAR) speckle, wavelet decomposition.**

I. Introduction

AFTER more than a half century since its inception as an imaging system in the 1950s and 1960s, there is still a growing interest in SAR imaging on account of its importance in a variety of applications such as high-resolution remote sensing for mapping, surface surveillance, search-and-rescue, mine detection, and automatic target recognition (ATR). SAR systems are currently employed in many airborne and satellite-borne platforms, such as the E-3 AWACS (Airborne Warning and Control System) airplane devoted to target tracking, the E-8C Joint STARS (Surveillance Target Attack Radar System) airplane performing target detection and localization, and the NASA space shuttle [1]. The one most important SAR attribute leading to its gain in popularity is the ability to image large areas of terrain at very fine resolutions and in all-weather conditions.

A major issue in SAR imagery is that basic textures are generally affected by multiplicative speckle noise [2]. Speckle noise is a consequence of image formation under coherent radiation. It is not truly a noise in the typical engineering sense, since its texture often carries useful information about the scene being imaged. However, the presence of speckle is generally considered undesirable since it damages radiometric resolution and it affects the tasks of human interpretation and scene analysis. Thus, it appears sensible to reduce speckle in SAR images, provided that the structural features and textural information are not lost.

Many adaptive filters for speckle reduction have been proposed in the past. The Frost filter was designed as an adaptive Wiener filter that assumed an autoregressive (AR) exponential model for the scene reflectivity [3]. Kuan considered a multiplicative speckle model and designed a linear filter based on the minimum mean-square error (MMSE) criterion, optimal when both the scene and the detected intensities are Gaussian distributed [4]. The Lee MMSE filter was a particular case of the Kuan filter based on a linear approximation made for the multiplicative noise model [5]. A two-dimensional (2-D) Kalman filter was developed by Sadjadi and Bannour under the modeling of the image as a Markov field satisfying a causal AR model [6]. The Gamma MAP filter was based on a Bayesian analysis of the image statistics where both signal and speckle noise follow a Gamma distribution [7]. Finally, a family of six robust filters for speckle reduction was proposed by Frery *et al.* employing trimmed maximum likelihood, best linear unbiased, and moment-based estimation, as well as median, interquartile range, and median absolute deviation [8].

Recently, there has been considerable interest in using the wavelet transform as a powerful tool for recovering SAR images from noisy data [9]–[12]. The main reason for the choice of multiscale bases of decompositions is that the statistics of many natural signals, when decomposed in such bases, are significantly simplified. When multiplicative contamination is concerned, multiscale methods involve a preprocessing step consisting of a logarithmic transform to separate the noise from the original image. Then, different wavelet shrinkage approaches are employed, which are based on Donoho's pioneering work [13]. More specifically, methods based on multiscale decompositions consist of three main steps: First, the raw data are decomposed by means of the wavelet transform, then the empirical wavelet coefficients are shrunk through a thresholding mechanism, and finally, the denoised signal is synthesized from the processed wavelet coefficients through the inverse wavelet transform. In [10], Gagnon and Jouan perform a comparative study between a complex wavelet coefficient shrinkage filter and several standard speckle filters that are largely used by SAR imaging scientists, and show that the wavelet-based approach is among the best for speckle removal.

Manuscript received July 9, 2002; revised March 6, 2003. The work of A. Achim was supported by the State Scholarships Foundation of Greece (IKY) under Grant 542/1999. The work of P. Tsakalides was supported in part by the Greek General Secretariat for Research and Technology under Program ΕΠΑΝ-M.4.3 Code 2013555 and 02ΠΡΑΞΕ47.

A. Achim and A. Bezerianos are with the Biosignal Processing Group, Medical Physics Department, University of Patras, 265 00 Rio, Greece (e-mail: AlinAchim@ieee.org; bezer@patreas.upatras.gr).

P. Tsakalides is with the Institute of Computer Science, FORTH and the Department of Computer Science, University of Crete, 714 09 Heraklion, Greece (e-mail: tsakalid@ics.forth.gr).

Digital Object Identifier 10.1109/TGRS.2003.813488

However, thresholding methods have two main drawbacks: i) the choice of the threshold, arguably the most important design parameter, is made in an *ad hoc* manner; and ii) the specific distributions of the signal and noise may not be well matched at different scales. To address these disadvantages, Simoncelli *et al.* developed nonlinear estimators, based on formal Bayesian theory, which outperform classical linear processors and simple thresholding estimators in removing noise from visual images [14], [15]. They used a generalized Laplacian model for the subband statistics of the signal and developed a noise-removal algorithm, which performs a "coring" operation to the data. In [16], Pizurica *et al.* proposed an efficient technique for despeckling SAR images by using analytic model distributions for the noise and signal wavelet coefficients. They developed a simple local model for spatial context and they obtained a family of adaptive shrinkage functions. Finally, Xie *et al.* developed a similar method by fusing the wavelet Bayesian denoising technique with Markov-random-field-based SAR image regularization [17].

It is recognized that parametric Bayesian processing presupposes proper modeling for the prior probability density function (PDF) of the signal [18]. In this paper, we show that a successful imaging algorithm can achieve both noise reduction and feature preservation if it employs a more accurate statistical description of the signal and noise components. Specifically, we demonstrate through extensive modeling of real data that the subband decompositions of SAR images have significantly non-Gaussian statistics that are best described by families of heavy-tailed distributions, such as the alpha-stable family. Consequently, we design a Bayesian estimator that exploits these statistics.

The innovative aspects of the present work consist of the following: i) In the data modeling component of our processor, we propose a new method for estimating the parameters of the alpha-stable distribution from noisy observations, which is based on Koutrouvelis' regression method [19]; ii) in the data filtering component of our processor, we select a uniform loss cost function for the design of the Bayes risk estimator, which results to a MAP filter based on alpha-stable statistics. Our design gives rise to a set of optimal nonlinear input-output processor curves parameterized by the degree of non-Gaussianity of the data.

The paper is organized as follows. In Section II, we provide some necessary preliminaries on alpha-stable processes and we present results on the modeling of the subband coefficients of actual SAR images indicating their heavy-tailed nature. In Section III, we present the design of our MAP estimator that exploits the signal alpha-stable statistics. In Section IV, the performance of our proposed algorithm is evaluated and compared with the performance of existing denoising methods. Finally, Section V concludes the paper and draws future work directions.

II. Modeling SAR Wavelet Coefficients With Alpha-Stable Distributions

This section is intended to provide an introduction on the alpha-stable statistical model used to characterize the wavelet subband coefficients of logarithmic transforms of actual SAR images. The model is suitable for describing signals that have highly non-Gaussian statistics and its parameters can be estimated from noisy observations. A review of the state of the art on stable processes from a statistical point of view is provided by a collection of papers edited by Cambanis, Samorodnitsky and Taqqu [20], while textbooks in the area have been written by Samorodnitsky and Taqqu [21], and by Nikias and Shao [22].

A. Basic Properties of the Alpha-Stable Family

The appeal of symmetric alpha-stable ($S\alpha S$) distributions as a statistical model for signals derives from some important theoretical and empirical reasons. First, stable random variables satisfy the stability property which states that linear combinations of jointly stable variables are indeed stable. Second, stable processes arise as limiting processes of sums of independent identically distributed (i.i.d.) random variables via the generalized central limit theorem. Actually, the *only* possible nontrivial limit of normalized sums of i.i.d. terms is stable. On the other hand, strong empirical evidence suggests that many datasets in several physical and economic systems exhibit heavy tail features that justify the use of stable models [23].

The $S\alpha S$ distribution is best defined by its characteristic function

$$\varphi(\omega) = \exp(j\delta\omega - \gamma|\omega|^{\alpha}) \tag{1}$$

where α is the *characteristic exponent*, taking values $0 < \alpha \leq 2$, δ $(-\infty < \delta < \infty)$ is the *location parameter*, and γ $(\gamma > 0)$ is the *dispersion* of the distribution. For values of α in the interval $(1, 2]$, the location parameter δ corresponds to the mean of the $S\alpha S$ distribution, while for $0 < \alpha \leq 1$, δ corresponds to its median. The dispersion parameter γ determines the spread of the distribution around its location parameter δ, similarly to the variance of the Gaussian distribution.

The characteristic exponent α is the most important parameter of the $S\alpha S$ distribution and it determines the shape of the distribution. The smaller the characteristic exponent α is, the heavier the tails of the $S\alpha S$ density. This implies that random variables following $S\alpha S$ distributions with small characteristic exponents are highly impulsive. Gaussian processes are stable processes with $\alpha = 2$ while Cauchy processes result when $\alpha = 1$. In fact, no closed-form expressions for the general $S\alpha S$ PDF are known except for the Gaussian and the Cauchy members.

Although the $S\alpha S$ density behaves approximately like a Gaussian density near the origin, its tails decay at a lower rate than the Gaussian density tails [21]. Indeed, let X be a non-Gaussian $S\alpha S$ random variable. Then, as $x \to \infty$

$$P(X > x) \sim c_{\alpha} x^{-\alpha} \tag{2}$$

where $c_{\alpha} = \Gamma(\alpha)(\sin(\pi\alpha/2))/\pi$, $\Gamma(x) = \int_0^{\infty} t^{x-1}e^{-t}\,dt$ is the Gamma function, and the statement $h(x) \sim g(x)$ as $x \to \infty$ means that $\lim_{x\to\infty} h(x)/g(x) = 1$. Hence, the tail probabilities are asymptotically power laws. In other words, while the Gaussian density has exponential tails, all other non-Gaussian stable densities have algebraic tails. Fig. 1 shows the tail behavior of several $S\alpha S$ densities including the Cauchy and the Gaussian. We should note that because expression (2) gives

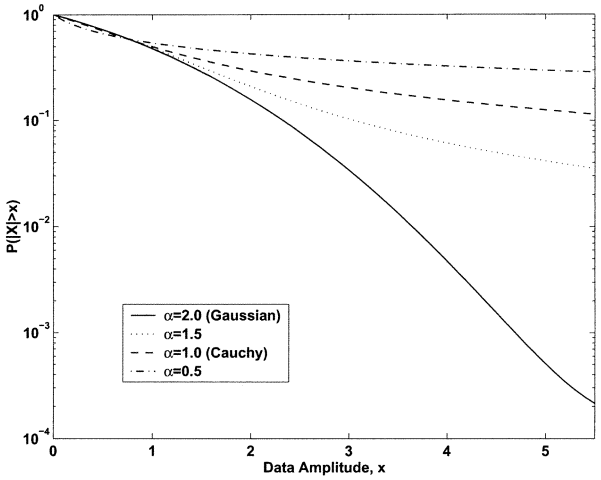

Fig. 1. $S\alpha S$ amplitude probability density functions for $\alpha = 0.5$, 1.0 (Cauchy), 1.5, and 2.0 (Gaussian). The dispersion parameter is kept constant at $\gamma = 1$.

exactly the tail probability of the Pareto distribution, the term "*stable Paretian laws*" is used to distinguish between the fast decay of the Gaussian law and the Pareto-like tail behavior when $\alpha < 2$.

The alpha-stable tail power law provided one of the earliest approaches in estimating the stability index α of real measurements [21]. The empirical distribution of the data, plotted on a log-log scale, should approach a straight line with slope $-\alpha$ if the data are stable. Another approach is based on quantiles [24]. Maximum likelihood (ML) methods developed by DuMouchel [25] and by Brorsen and Yang [26] are asymptotically efficient but were considered difficult to compute. Recently, Nolan showed that ML estimation of stable parameters is feasible by designing an efficient program [27].

One consequence of heavy tails is that only moments of order less than α exist for the non-Gaussian alpha-stable family members, i.e.,

$$E|X|^p < \infty \qquad \text{for } p < \alpha. \tag{3}$$

As a result, stable Paretian laws have infinite variance. In the past, the infinite variance property of the $S\alpha S$ family has caused skeptics to dismiss the stable model. With the same reasoning, one could argue that the routinely used Gaussian distribution, which has infinite support, should also be dismissed as a model of bounded measurements. In practice, one should remember that it is important to capture the shape of the distribution and that the variance is only one measure of the spread of a density [27].

B. Alpha-Stable Modeling of Radar Reflectivity Wavelet Coefficients

In this section, we show results on modeling data obtained by applying the 2-D wavelet transform to a set of real SAR images. The wavelet transform expands a signal using a set of basis functions, which are obtained from a single prototype function called the "mother wavelet." The result of the expansion is a sequence of signal approximations at successively coarser resolutions. The so-called "detail signal" is the difference in information between approximations at two consecutive resolutions, and it can be represented by another series expansion. If we consider an original 2-D signal of size $N \times N$, N usually being a power of $2(N = 2^j)$, such a decomposition scheme is mathematically referred to as the *dyadic wavelet transform* (DWT). In image processing applications, the above scheme is applied along both the abscissa and the ordinate. Thus, the DWT decomposes images with a multiresolution scale factor of two, providing at each resolution level one low-resolution approximation and three spatially oriented wavelet details [28], [29]. In the past, several authors have pointed out that, in a subband representation of images, histograms of wavelet coefficients have heavier tails and more sharply peaked modes at zero than what is assumed by the Gaussian distribution [15], [29], [30]. Here, we study whether the stable family provides a flexible and appropriate tool for modeling the coefficients within the framework of multiscale wavelet analysis of logarithmically transformed SAR images.

To achieve this goal, we modeled a series of SAR images from the MSTAR Public Clutter dataset.[1] The dataset contains X-band images with 1784 $\times$ 1476 pixels and 1 ft $\times$ 1 ft resolution at 15° depression angles. Since speckle appears inherently in any SAR image, we have first processed the actual images using the Gamma-MAP filter [7] and considered the resulting images as reasonable approximations of the speckle free radar reflectivity. Because of limited space, in this paper we describe the modeling of ten representative images in intensity format. All of them have a 256 gray-level resolution and constitute cropped versions (512 $\times$ 512 pixels) of the original images.

We proceed in two steps. First, we assess whether the data deviate from the normal distribution and if they have heavy tails. To determine that, we make use of normal probability plots. Then, we check if the data is in the stable domain of attraction by estimating the characteristic exponent, α, directly from the data and by providing the related confidence intervals. Several methods have been proposed for estimating stable parameters. Here, we use the maximum likelihood method described by Nolan in [27], which gives reliable estimates and provides the most tight confidence intervals. As further stability diagnostics, we employ probability density plots that give a good indication of whether the $S\alpha S$ fit matches the data near the mode and at the tails of the distribution.

In Fig. 2, we show the filtered image HB06158 from the MSTAR collection, its log-transformed version and the corresponding three-scale decomposition. The normal probability plot corresponding to the vertical subband at the first level of decomposition of this image is shown in Fig. 3. The plot provides strong evidence that the underlying distribution is not normal. The "+" marks in the plot show the empirical probability versus the data value for each point in the sample. The marks are in a curve that does not follow the straight Gaussian line and thus, the normality assumption is violated for this data. While non-Gaussian stable densities are heavy-tailed, not all heavy-tailed distributions are stable. Hence, in Fig. 4

[1]The dataset can be obtained through the Sensor Data Management System (SDMS) of Wright Laboratory at the URL http://www.mbvlab.wpafb.af.mil/public/sdms/.

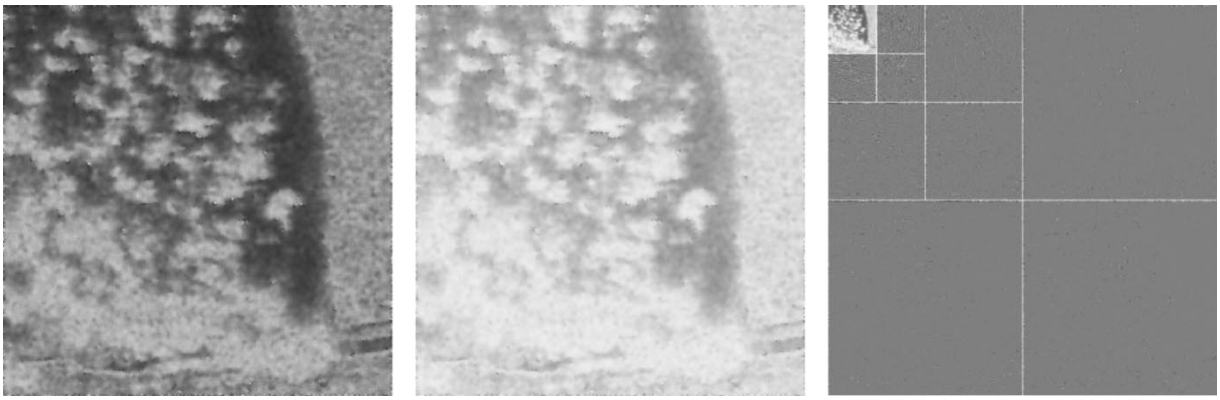

(a) (b) (c)

Fig. 2. (a) Filtered image HB06158, (b) its log-transformed version, and (c) the corresponding three-scale wavelet decomposition.

we assess the stability of the data. First, the characteristic exponent is estimated and the data sample is fitted with the corresponding stable distribution. For the particular case shown here, the characteristic exponent of the $S\alpha S$ distribution which best fits the data was estimated to be $\hat{\alpha} = 1.253$. The stabilized p-p $S\alpha S$ plot in Fig. 4 shows a highly accurate stable fit for this dataset.

Naturally, the real question is whether the stable fit describes the data more accurately than other PDF functions proposed in the literature. Here, we compare the $S\alpha S$ fits with those provided by the generalized Laplacian (or generalized Gaussian) density function proposed by Mallat in [29] and also used by Simoncelli in [14] and [15]

$$f_{s,\,p}(c) = \frac{e^{-|c/s|^p}}{Z(s,p)} \tag{4}$$

where $Z(s,\,p) = 2\,(s/p)\Gamma(1/p)$. The parameters s and p can be computed from the second and fourth moments of the data

$$\sigma^2 = \frac{s^2\Gamma\left(\frac{3}{p}\right)}{\Gamma\left(\frac{1}{p}\right)} \quad k = \frac{\Gamma\left(\frac{1}{p}\right)\Gamma\left(\frac{5}{p}\right)}{\Gamma^2\left(\frac{3}{p}\right)} \tag{5}$$

where σ^2 is the distribution variance, and k is the kurtosis. In order to model the wavelet subband coefficients of images, one can examine their histograms [14], [18], [29], which model their probability density functions or equivalently use amplitude probability density (APD) functions $(P|X| > x)$. The APD can be evaluated empirically directly from the data, as well as theoretically from the density function considered. Fig. 5 shows an example of modeling the vertical subband at the first level of decomposition of the SAR image under study. A highly accurate stable fit can be observed. In particular, the figure shows that the $S\alpha S$ distribution is superior to the generalized Laplacian distribution because it provides a better fit to both the mode and the tails of the empirical density of the actual data.

For every image we iterated three times the separable wavelet decomposition and we modeled the coefficients of each subband by using the $S\alpha S$ family. The wavelet decomposition was accomplished using Daubechies' Symmlet 8 basis wavelet. The results are summarized in Table I, which shows the ML estimates of the characteristic exponent α together with the corresponding 95% confidence intervals. It can be observed that the

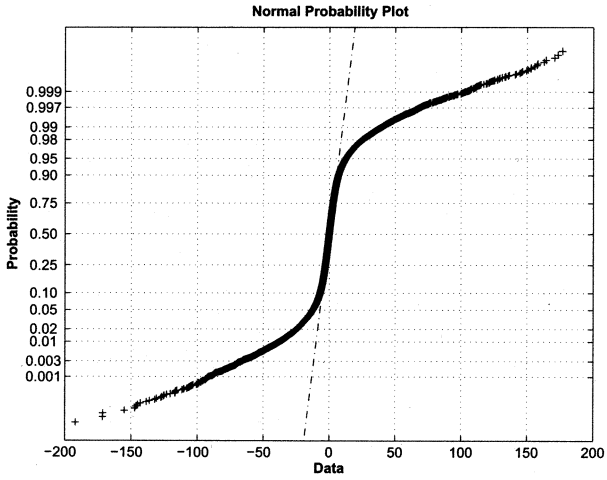

Fig. 3. Normal probability plot of the vertical subband at the first level of decomposition of filtered image HB06158 from MSTAR dataset. Characterization of data non-Gaussianity. The "+" marks correspond to the empirical probability density versus the data value for each point in the sample. Since the marks are in a curve that does not follow the straight Gaussian line, the normality assumption is violated for this data.

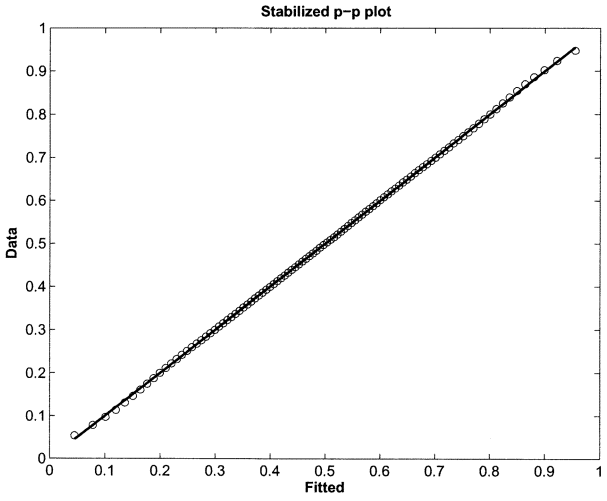

Fig. 4. Stabilized p-p plot for $S\alpha S$ fit of dataset representing the vertical subband at the first level of decomposition of filtered image HB06158. The "o" marks, denoting the empirical probability density, are in a curve that very accurately follows the straight $S\alpha S$ line corresponding to $\alpha = 1.253$.

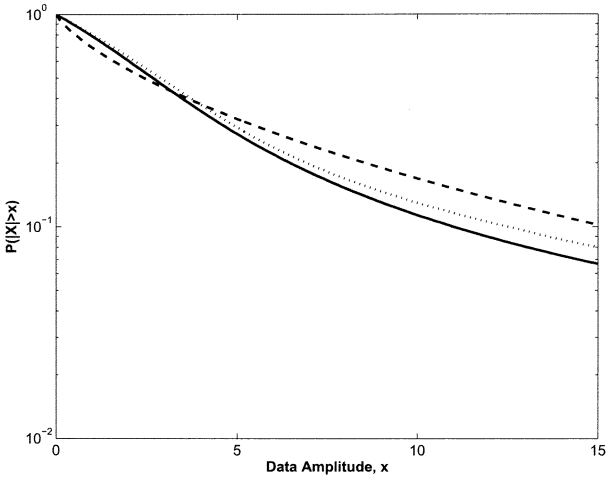

Fig. 5. Modeling of the vertical subband at the first level of decomposition of filtered image HB06158 with the $S\alpha S$ and the generalized Laplacian density functions, depicted in solid and dashed lines, respectively. The $S\alpha S$ distribution has characteristic exponent $\alpha = 1.253$ and dispersion $\gamma = 0.0350$ while the generalized Laplacian has parameters $p = 0.419$ and $s = 0.0434$ [cf. (4)]. The dotted line denotes the empirical APD.

confidence interval depends on the particular level of decomposition. The confidence interval becomes wider as the level increases since the number of samples used for estimating α gets smaller. The table demonstrates that the coefficients of different subbands and decomposition levels exhibit various degrees of non-Gaussianity. The important observation is that all subbands exhibit distinctly non-Gaussian characteristics, with values of α varying between 0.7 and 1.9, away from the Gaussian point of $\alpha = 2$. Our modeling results clearly point to the need for the design of Bayesian processors that take into consideration the non-Gaussian heavy-tailed character of the radar reflectivity to achieve close to optimal speckle mitigation performance.

TABLE I
ALPHA-STABLE MODELING OF WAVELET SUBBAND COEFFICIENTS OF ACTUAL SAR IMAGES FROM THE MSTAR PUBLIC CLUTTER DATASET. MAXIMUM LIKELIHOOD PARAMETER ESTIMATES AND 95% CONFIDENCE INTERVALS FOR THE $S\alpha S$ CHARACTERISTIC EXPONENT, α. THE TABULATED KEY PARAMETER α DEFINES THE DEGREE OF NON-GAUSSIANITY AS DEVIATIONS FROM THE VALUE $\alpha = 2$, WHICH CORRESPONDS TO THE GAUSSIAN CONDITION

IMAGE	Level	Image Subbands		
		Horizontal	Vertical	Diagonal
HB06158	I	1.232 ± 0.010	1.253 ± 0.010	0.812 ± 0.009
HB06159		1.336 ± 0.011	1.362 ± 0.010	0.867 ± 0.008
HB06160		1.014 ± 0.009	1.042 ± 0.010	0.686 ± 0.007
HB06161		1.064 ± 0.009	1.094 ± 0.009	0.703 ± 0.007
HB06162		1.048 ± 0.009	1.058 ± 0.009	0.709 ± 0.007
HB06163		1.084 ± 0.010	1.084 ± 0.010	0.718 ± 0.007
HB06215		1.371 ± 0.011	1.367 ± 0.011	0.885 ± 0.007
HB06245		1.286 ± 0.010	1.300 ± 0.010	0.850 ± 0.008
HB06246		1.308 ± 0.011	1.315 ± 0.010	0.844 ± 0.007
HB06278		1.231 ± 0.011	1.242 ± 0.011	0.807 ± 0.007
HB06158	II	1.395 ± 0.022	1.442 ± 0.022	1.032 ± 0.019
HB06159		1.492 ± 0.022	1.527 ± 0.023	1.029 ± 0.018
HB06160		1.215 ± 0.021	1.253 ± 0.022	0.963 ± 0.020
HB06161		1.269 ± 0.021	1.293 ± 0.021	0.944 ± 0.019
HB06162		1.248 ± 0.021	1.277 ± 0.022	0.961 ± 0.019
HB06163		1.256 ± 0.022	1.295 ± 0.022	0.968 ± 0.020
HB06215		1.516 ± 0.022	1.525 ± 0.021	1.073 ± 0.019
HB06245		1.422 ± 0.022	1.437 ± 0.021	1.053 ± 0.019
HB06246		1.447 ± 0.022	1.468 ± 0.021	0.993 ± 0.017
HB06278		1.365 ± 0.021	1.394 ± 0.021	0.993 ± 0.018
HB06158	III	1.684 ± 0.045	1.688 ± 0.043	1.578 ± 0.043
HB06159		1.667 ± 0.045	1.817 ± 0.040	1.513 ± 0.044
HB06160		1.456 ± 0.045	1.660 ± 0.046	1.543 ± 0.047
HB06161		1.567 ± 0.047	1.685 ± 0.043	1.542 ± 0.046
HB06162		1.614 ± 0.044	1.627 ± 0.045	1.556 ± 0.047
HB06163		1.705 ± 0.047	1.626 ± 0.048	1.486 ± 0.047
HB06215		1.883 ± 0.034	1.776 ± 0.042	1.576 ± 0.044
HB06245		1.659 ± 0.046	1.863 ± 0.041	1.594 ± 0.044
HB06246		1.704 ± 0.043	1.683 ± 0.042	1.515 ± 0.042
HB06278		1.568 ± 0.045	1.620 ± 0.044	1.568 ± 0.045

III. WAVELET-BASED IMAGE-DENOISING NONLINEAR SAR PROCESSOR

In this Section, our goal is the design of a formal Bayesian estimator that recovers the signal component of the wavelet coefficients in SAR images by using an alpha-stable signal prior distribution. The proposed processor is motivated by the modeling studies in the previous section, it is based on solid statistical theory, and it does not depend on the use of *ad hoc* thresholding parameters.

In order to be able to implement a MAP processor, one should first estimate the parameters of the prior distributions of the signal and noise components of the measurements. The signal component is modeled according to a $S\alpha S$ distribution with zero location parameter, while, as we present in the following, the noise component can be modeled as a zero-mean Gaussian random variable.

A. Problem Formulation and Speckle Noise Model

Denote by $I(x, y)$ a noisy observation (i.e., the recorded SAR image) of the 2-D function $S(x, y)$ (i.e., the noise-free SAR image that has to be recovered) and by $\eta_m(x, y)$ and $\eta_a(x, y)$ the corrupting multiplicative and additive speckle noise components, respectively. One can write

$$I(x, y) = S(x, y) \cdot \eta_m(x, y) + \eta_a(x, y), \qquad (x, y) \in \mathbf{Z}^2. \tag{6}$$

Generally, the effect of the additive component of the speckle in SAR images is less significant than the effect of the multiplicative component. Thus, ignoring the term $\eta_a(x, y)$, one can rewrite (6) as

$$I(x, y) = S(x, y) \cdot \eta_m(x, y). \tag{7}$$

The statistical properties of speckle noise $\eta_m(x, y)$ were studied by Goodman [2]. He has shown that, if the number of scatterers per resolution cell is large, a fully developed speckle pattern can be modeled as the magnitude of a complex Gaussian field with i.i.d. real and imaginary components. Arsenault and April [31] have shown that when the image intensity is logarithmically transformed, the speckle noise is approximately Gaussian additive noise, and it tends to a normal probability much faster than the intensity distribution. Xie *et al.* employ a distance between cumulative distributions to measure the deviation of the log-transformed speckle from Gaussianity [32]. They confirm the result in [31] and show that even for the amplitude image, although the log-transformed speckle tends to

a Gaussian PDF slightly slower than the original speckle noise, the former is still statistically very close to the Gaussian PDF.

Other realistic speckle noise models include the K-distribution [33], $\mathcal{G}$-distribution [34], log-normal distribution [10], and correlated speckle pattern [18], [33]. However, since our processor employs the wavelet transform which, through the central limit theorem, drives the noise wavelet coefficients to approximate a Gaussian distribution, we use the *log-normal* distribution as the speckle noise model. If X follows the log-normal distribution with parameters μ and σ^2, then $\ln X$ follows the normal distribution with mean μ and variance σ^2. For the log-normal distribution, the mean and variance are given, respectively, by

$$M = \exp\left(\mu + \frac{\sigma^2}{2}\right) \tag{8}$$

$$\sigma_{\ln}^2 = \exp\left(2\mu + 2\sigma^2\right) - \exp\left(2\mu + \sigma^2\right). \tag{9}$$

The appropriateness of the use of the log-normal model for speckle noise has also been assessed by Kaplan [35]. A log-normal random variable can be generated using

$$X_{\log\text{-normal}} = \exp\left(X_{\text{normal}}\sqrt{2\log\frac{M}{m}} + \ln m\right) \tag{10}$$

where M and m are the mean and the median values of the distribution, respectively, and X_{normal} is a standard zero-mean, unit-variance Gaussian random variable. There is a straightforward equivalence between the equivalent number of looks (ENL) in a speckle image and the parameter m in the above expression [10].

B. Parameter Estimation in the Wavelet Domain

Based on the above description of the speckle effect, it is sensible to transform the multiplicative noise model into an additive one by taking the logarithm of the original speckled data

$$\log I(x, y) = \log S(x, y) + \log \eta_m(x, y). \tag{11}$$

Expression (11) can be rewritten as

$$f(x, y) = g(x, y) + \epsilon(x, y) \tag{12}$$

where $f(\cdot)$, $g(\cdot)$, and $\epsilon(\cdot)$ are the logarithms of $I(\cdot)$, $S(\cdot)$, and $\eta_m(\cdot)$, respectively. In (12), we assume that the signal and noise components are independent random variables.

At this stage, one can consider $\epsilon(x, y)$ to be white noise and subsequently apply any conventional additive noise suppression technique, such as Wiener filtering. However, it is recognized that standard noise filtering methods often result in blurred image features. Indeed, single-scale representations of signals, either in time or in frequency, are often inadequate when attempting to separate signals from noisy data. The wavelet transform has been proposed as a useful processing tool for signal recovery [28], [36].

The wavelet transform is a linear operation. Consequently, after applying the DWT to (12) we get, at each resolution level and for all orientations, sets of noisy wavelet coefficients written as the sum of the transformations of the signal and the noise

$$d_{j,k}^i = s_{j,k}^i + \xi_{j,k}^i \tag{13}$$

where $k = 0, \ldots, 2^{J+j} - 1$ and $-1 < j < -J$ refer to the decomposition level or scale and $i = 1, 2, 3$ refers to the three spatial orientations.

In a Bayesian framework, referring to (13), $d_{j,k}$, $s_{j,k}$, and $\xi_{j,k}$ are considered as samples of the random variables d, s, and ξ, respectively. The distribution parameters corresponding to the signal (s) and noise wavelet coefficients (ξ) should be estimated from the noisy observations (d) in an efficient manner. To achieve this, we observe that the PDF of the measured coefficients is the convolution between the PDFs of the signal and noise components. Consequently, the associated characteristic function of the measurements is given by the product of the characteristic functions of the signal and noise

$$\Phi_d(\omega) = \Phi_s(\omega) \cdot \Phi_\xi(\omega). \tag{14}$$

Motivated by the modeling analysis in Section II-B, a $S\alpha S$ density is chosen for the signal component

$$\Phi_s(\omega) = \exp\left(-\gamma_s|\omega|^{\alpha_s}\right), \qquad 0 < \alpha \leq 2$$

while a Gaussian distribution characterizes the noise component

$$\Phi_\xi(\omega) = \exp\left(-\frac{\sigma^2}{2}|\omega|^2\right).$$

At this point, we observe that (14) implies that

$$\log\left[-\left(\log|\Phi_d(\omega)|^2 + \sigma^2\omega^2\right)\right] = \log(2\gamma_s) + \alpha_s \log|\omega|. \tag{15}$$

First, we estimate the level of noise. As proposed in [13], a robust estimate of the noise standard deviation, σ, is obtained in the finest decomposition scale by the measured wavelet coefficients as

$$\hat{\sigma} = \frac{1}{0.6745}\,\text{MAD}\left(\left\{d_{J,k},\, 0 \leq k < 2^J\right\}\right) \tag{16}$$

where MAD signifies the *median absolute deviation* operator and J denotes the finest level of wavelet decomposition. Then, we find the parameters α_s and γ_s by regressing $y = \log[-(\log|\Phi_d(\omega)|^2 + \sigma^2\omega^2)]$ on $w = \log|\omega|$ in the model

$$y_k = \mu + \alpha\, w_k + \epsilon_k \tag{17}$$

where $\mu = \log(2\gamma)$, ϵ_k denotes an error term, and $(\omega_k,\, k = 1, \ldots, K)$ is an appropriate set of real numbers. The optimum number K of points depends on the characteristic exponent α and on the sample size. Specifically, K decreases as α increases and as the number of samples increases. For a more detailed discussion on choosing the optimal K, please see [19].

We found that this method for estimating the $S\alpha S$ parameters gives reliable estimates, it is computationally efficient and, more importantly, it allows us to estimate the parameters from the noisy measurements. Koutrouvelis in [19] used a similar approach to estimate the parameters of alpha-stable distributions and he showed that his regression method gives very good results in terms of consistency, bias, and efficiency.

C. MAP Processor for SAR Speckle Removal

Having estimated the necessary signal and noise distribution parameters from the data, our goal is to design and implement a Bayes risk processor. The Bayes estimator $\hat{s}$ minimizes the

conditional risk, which is the loss averaged over the conditional distribution of s, given the noisy observation, d

$$\hat{s}(d) = \arg\min_{\hat{s}} \int L[s,\, \hat{s}(d)]\, P_{s|d}(s\,|d)\, ds. \tag{18}$$

Selecting the uniform cost function

$$L[s,\, \hat{s}(d)] = \begin{cases} 0, & \text{for } |s - \hat{s}| < \epsilon \\ 1, & \text{otherwise} \end{cases} \tag{19}$$

the optimal estimator can be derived as follows:

$$\begin{aligned} \hat{s}(d) &= \arg\min_{\hat{s}} \int_{|s-\hat{s}| \geq \epsilon} P_{s|d}(s\,|d)\, ds \\ &= \arg\min_{\hat{s}} \left[1 - \int_{|s-\hat{s}|<\epsilon} P_{s|d}(s\,|d)\, ds \right]. \end{aligned} \tag{20}$$

Thus, in order to minimize the expected cost, when $\epsilon \to 0$ one should select

$$\hat{s}(d) = \arg\max_{\hat{s}} P_{s|d}(s\,|d). \tag{21}$$

It is important to underline at this point that under the loss function in (19), the estimator given by expression (18) is well defined for all $S\alpha S$ random variables (with characteristic exponent α taking values in the whole range $0 < \alpha \leq 2$). This estimator is called the maximum *a posteriori* (MAP) estimator. Bayes' theorem gives the *a posteriori* PDF of s based on the measured data

$$P_{s|d}(s\,|d) = \frac{P_{d|s}(d\,|s)\, P_s(s)}{P_d(d)} \tag{22}$$

where $P_s(s)$ is the *prior* PDF of the alpha-stable modeled signal component of the measurements and $P_{d|s}(d\,|s)$ is the *likelihood* function. Substituting (22) in (21), we get

$$\begin{aligned} \hat{s}(d) &= \arg\max_{\hat{s}} P_{d|s}(d\,|s)\, P_s(s) = \arg\max_{\hat{s}} P_\xi(d-s) P_s(s) \\ &= \arg\max_{\hat{s}} P_\xi(\xi) P_s(s). \end{aligned} \tag{23}$$

Only for the case of Gaussian signal and Gaussian noise does a closed-form solution exist for the processor described above

$$\hat{s}(d) = \frac{\sigma_s^2}{\sigma_s^2 + \sigma^2}\, d \tag{24}$$

where σ_s^2 is the Gaussian signal variance. In other words, the processing is a simple linear rescaling of the measurement. For the general alpha-stable signal case, the Bayesian processor does not have a closed-form expression and one has to numerically compute the MAP input-output curves. We will refer to the new algorithm as the Wavelet-Based Image-Denoising Nonlinear SAR (WIN-SAR) processor. A functional block diagram of the WIN-SAR processor is shown in Fig. 6. We should note here that due to the use of the logarithmic transformation, the mean of the log-transformed speckle field is biased [32]. For unit-mean log-normal distributed speckle noise, the mean of the corresponding Gaussian distribution is equal to minus half of its variance [cf. (8)]. Therefore, as proposed by Xie *et al.* [17], this biased mean should be corrected by adding an additional step "adjust mean" between the "IDWT" and the "EXP" modules of our processor (cf. Fig. 6).

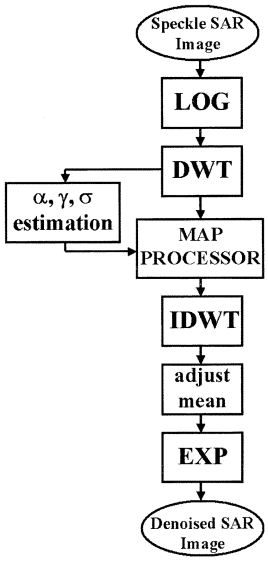

Fig. 6. Block diagram of the proposed multiscale homomorphic Bayesian-based WIN-SAR algorithm for speckle suppression. Our proposed novel wavelet coefficient statistical characterization and MAP processing modules result in a more accurate SAR image reconstruction.

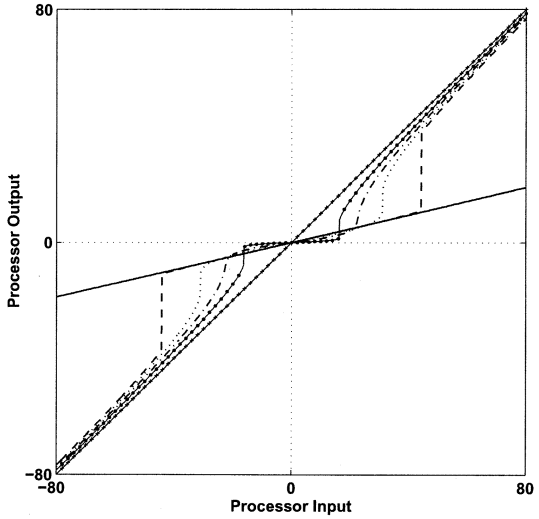

Fig. 7. WIN-SAR processor input-output curves for alpha-stable signal and Gaussian noise prior distributions. The straight line with xs indicates the identity function. The five different signal statistics correspond to $\alpha = 2$ (Gaussian signal, solid line), $\alpha = 1.95$ (slightly non-Gaussian signal, dashed line), $\alpha = 1.5$, $\alpha = 1$, and $\alpha = 0.5$ (considerably heavy-tailed signal, dotted, dash-dotted and solid with $\circ$ lines, respectively). All the curves correspond to a same ratio $\sigma/\gamma = 2$.

Fig. 7 depicts the numerically computed WIN-SAR input-output curves for five different values of the signal characteristic exponent, α, namely, $\alpha = 2$ (Gaussian data), $\alpha = 1.95$ (slightly non-Gaussian data), $\alpha = 1.5$, $\alpha = 1$, and $\alpha = 0.5$ (considerably heavy-tailed data). Apart from the case $\alpha = 2$, all curves correspond to a nonlinear "coring" operation, i.e., large-amplitude observations are essentially preserved while small-amplitude values are suppressed. This is expected since small measurement values are assumed to come from signal values close to zero. Fig. 7 also illustrates the WIN-SAR processor dependency on the parameter α of the signal prior PDF. Specifically, for a given ratio γ_s/σ, the amount of shrinkage decreases as α

Fig. 8. Results of various speckle suppressing methods. (Top to bottom) Original, noisy (ENL $= 8$), GMAP-filtered, soft thresholding, and WIN-SAR denoised images, respectively. (Left to right) Aerial image, boat image, Brodatz textures.

decreases. The intuitive explanation for this behavior is that the smaller the value of α, the heavier the tails of the signal PDF and the greater the probability that the measured value is due to the signal.

IV. Experimental Results

In this section, we present simulation results obtained by processing several test SAR images using our proposed WIN-SAR speckle suppression processor and we compare the results of our approach with other current state-of-the-art speckle filtering methods. In order to be able to quantify the improvement achieved by our method, we have first degraded three original "noiseless" images with synthetic speckle in a controlled manner. Finally, for qualitative visual evaluation, we processed various unaltered SAR images with WIN-SAR.

A. Synthetic Data Examples

We were interested in performing experiments on images of different types and with various content in order to be able to obtain results, which we could claim to be general enough (Fig. 8). Thus, an aerial image was used for its identical content with real SAR images. This image was obtained by cropping "*westaerialconcorde*" found in Matlab's Image Processing Toolbox. For testing the smoothing performance of the algorithm as well as its edge preservation potential, we also chose to apply it on the classical "*boat*" image. Finally, as a test for texture preservation, we generated an image containing four different textures and applied the algorithms to it. In order to obtain speckle images, we degraded the original test images by multiplying them with unit-mean random fields, defined in expression (10). In our experiments, we considered three different levels of simulated speckle noise, with ENL $= 1$, 3, and 8, respectively.

We compared the results of our approach with other speckle reduction techniques including the Lee filter [5], the GMAP filter [7], and wavelet shrinkage denoising using soft thresholding [13]. We selected the parameters associated with each method by trial-and-error in order to achieve optimal results. Specifically, for the Lee filter we used a 5×5 mask, while the GMAP filter was implemented using a window of size 7×7 pixels. For soft thresholding, we used a threshold $t = 1.5\,\sigma_d$, σ_d being the standard deviation of the wavelet coefficients. The wavelet shrinkage soft thresholding scheme was implemented using Daubechies' Symmlet 8 mother wavelet. In order to minimize side effects like pseudo-Gibbs phenomena, we embedded both wavelet-based methods (including our Bayesian approach) into the cycle spinning algorithm [37]. This algorithm was implemented using 8 circulant shifts of the input image. The parameters α_s and γ_s in the WIN-SAR processor are estimated for each shift. The maximum number of wavelet decompositions we used was 5.

In order to quantify the achieved performance improvement, three different measures were computed based on the original and the denoised data. For quantitative evaluation, an extensively used measure is the MSE defined as

$$\text{MSE} = \frac{1}{K}\sum_{i=1}^{K}(\hat{S}_i - S_i)^2 \tag{25}$$

where S is the original image, $\hat{S}$ is the denoised image, and K is the image size. Also, in order to quantify the speckle reduction performance we computed the standard-deviation-to-mean ratio (S/M). This quantity is a measure of image speckle in homogeneous regions.

Remember that in SAR imaging, we are interested in suppressing speckle noise while at the same time preserving the edges of the original image that often constitute features of interest. Thus, in addition to the above quantitative performance measures, we also considered a qualitative measure for edge preservation. More specifically, we used a parameter β originally defined in [38]

$$\beta = \frac{\Gamma\left(\Delta S - \overline{\Delta S}, \widehat{\Delta S} - \overline{\widehat{\Delta S}}\right)}{\sqrt{\Gamma\left(\Delta S - \overline{\Delta S}, \Delta S - \overline{\Delta S}\right)\cdot\Gamma\left(\widehat{\Delta S} - \overline{\widehat{\Delta S}}, \widehat{\Delta S} - \overline{\widehat{\Delta S}}\right)}} \tag{26}$$

where ΔS and $\widehat{\Delta S}$ are the highpass-filtered versions of S and $\hat{S}$, respectively, obtained with a 3×3-pixel standard approxima-

TABLE II
IMAGE ENHANCEMENT MEASURES OBTAINED BY FOUR DENOISING METHODS APPLIED ON THE "AERIAL," "BOAT," AND "TEXTURE" TEST IMAGES. THREE LEVELS OF NOISE ARE CONSIDERED CORRESPONDING TO ENL $= 1, 3$, AND 8. THE MEASURES ARE CALCULATED ON AN AVERAGE OF TEN NOISE REALIZATIONS

	ENL $= 1$			ENL $= 3$			ENL $= 8$		
Method	MSE	S/M	β	MSE	S/M	β	MSE	S/M	β
Aerial									
Noisy	133.008	1.1160	0.0091	76.9237	0.7090	0.1530	47.1145	0.5186	0.2475
Lee	43.0164	0.4696	0.0641	28.0031	0.3915	0.1671	19.7911	0.3639	0.3293
GMAP	49.7448	0.5079	0.0465	25.9859	0.3831	0.1644	18.1121	0.3572	0.3212
Soft Thresh	26.0327	0.3633	0.1733	19.9360	0.3446	0.2742	16.0158	0.3384	0.4153
WIN-SAR	22.6918	0.3542	0.2975	17.9175	0.3503	0.3572	15.2902	0.3519	0.4465
Boat									
Noisy	146.663	1.1236	0.0071	84.7040	0.7249	0.1260	51.8864	0.5360	0.2064
Lee	46.0288	0.4908	0.0692	29.6245	0.4224	0.2025	20.1947	0.3964	0.3723
GMAP	54.2931	0.5317	0.0582	27.2822	0.4116	0.1830	18.1902	0.3879	0.3563
Soft Thresh	27.0723	0.3990	0.1993	19.4914	0.3806	0.3136	14.5934	0.3743	0.4692
WIN-SAR	21.9034	0.3796	0.3930	16.0180	0.3783	0.4683	12.9552	0.3784	0.5655
Texture									
Noisy	137.948	1.3221	0.01913	79.8702	0.9111	0.3216	48.8696	0.7363	0.4879
Lee	54.8546	0.6383	0.1269	38.7003	0.5893	0.3463	29.5721	0.5998	0.5458
GMAP	56.7328	0.7029	0.1789	39.6036	0.6302	0.2942	28.8340	0.5901	0.5762
Soft Thresh	40.9577	0.5439	0.3283	33.4261	0.5821	0.5070	27.4575	0.5886	0.6115
WIN-SAR	38.5930	0.6183	0.3957	31.5617	0.5442	0.5177	25.0375	0.5513	0.6498

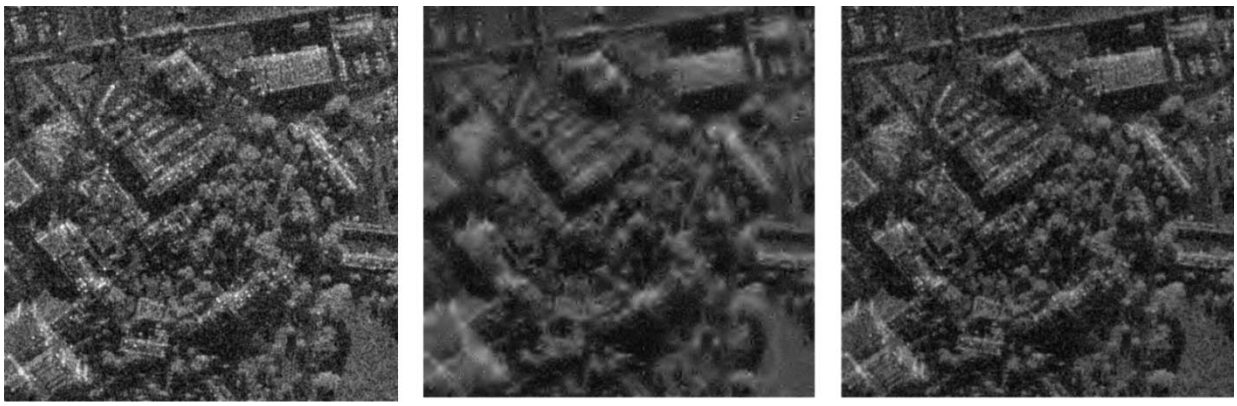

(a) (b) (c)

Fig. 9. Processing of SAR image of urban scene. (a) Original SAR image. (b) Image denoised using soft thresholding. (c) Image enhanced using WIN-SAR algorithm.

tion of the Laplacian operator, the overline operator represents the mean value, and

$$\Gamma(S_1, S_2) = \sum_{i=1}^{K} S_{1_i} \cdot S_{2_i}. \tag{27}$$

The correlation measure, β should be close to unity for an optimal effect of edge preservation.

The obtained values of MSE, S/M, and β for all methods applied to the three test images are given in Table II. The numbers in the table represent average values obtained after repeating each experiment ten times, using the same settings but for different noise realizations. It is evident from the table that the two wavelet-based methods are more successful in speckle noise suppression than the Lee and GMAP filters in most situations. It can be seen that in general our proposed WIN-SAR processor exhibits the best performance according to all three metrics. The soft thresholding method occasionally gives better results in terms of the S/M measure but at the expense of over-smoothed images as it can be seen by comparing the β index metric as well as by visual inspection of Fig. 8. In terms of MSE, the soft thresholding scheme achieves comparable performance with the GMAP filter, but the visual quality of the soft threshold processed images seems to be better. This is due to the fact that the soft thresholding approach is not intended to minimize the MSE, the result being an estimator which achieves a low variance at the expense of bias [13]. Observing the β metric values, we see that our WIN-SAR multiresolution technique exhibits a clearly better performance in terms of edge preservation, as expected.

B. Real SAR Imagery Examples

The problem with the MSE, S/M, and β measures, or with any other metric, is associating them directly to the visual interpretation of a human observer. Hence, in order to study the merit of the proposed $S\alpha S$ subband coefficient modeling and the resulting WIN-SAR processor, we also chose noisy SAR images, we applied the algorithm without adding artificial noise, and we visually evaluated the denoised images. The first test image (single-look, amplitude format), shown in Fig. 9(a), depicts an urban scene having a dense set of large cross-section targets with intermingled tree shadows. This image was provided by D. E. Wahl (Sandia National Laboratories), and it was also used in [39].

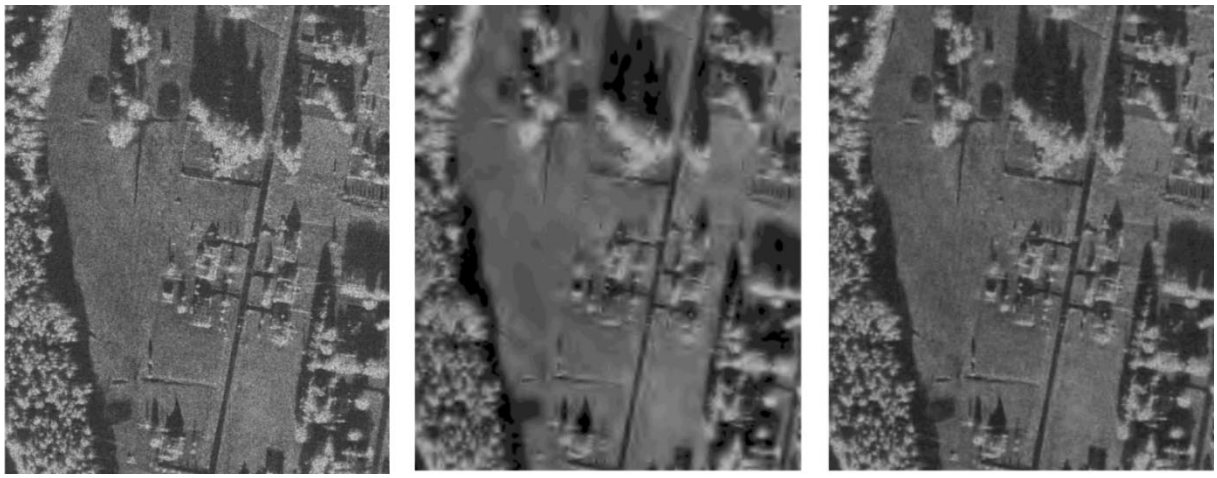

(a) (b) (c)

Fig. 10. Processing of a clutter-like scene. (a) Noisy SAR image. (b) Image denoised using soft thresholding. (c) Image enhanced using WIN-SAR algorithm.

We should note at this point that in situations where the image is affected by speckle with a high correlation length, algorithmic design should account for noise correlation and a whitening filter should be used. Alternatively, the data could be downsampled at the cost of reducing the spatial resolution. The use of an orthonormal wavelet basis guarantees that the noise component of the wavelet coefficients will be uncorrelated, provided that the noise was white in the image domain. The second test image shown in Fig. 10(a) illustrates this idea. The image represents a rural scene from the MSTAR collection. The results shown in Fig. 10 are obtained after downsampling the original image by a factor of 2.

For visual comparison, we show results obtained using the soft thresholding based scheme [Figs. 9(b) and 10(b)] and the WIN-SAR processor [Figs. 9(c) and 10(c)]. Although qualitative evaluation in these cases is highly subjective, i.e., no universal quality measure for filtered SAR data exists, the results of the above two experiments seem to be consistent with the simulation results. The soft thresholding method achieves good speckle suppression performance but it over-smoothes images and thus many features are blurred. It appears that the proposed WIN-SAR processor performs like a feature detector, retaining the features that are clearly distinguishable in the speckled data while filtering out anything which is assumed to be constituted by noise.

V. Conclusion

We introduced a new statistical representation for the wavelet decomposition coefficients of SAR images, based on heavy-tailed alpha-stable models. Consequently, we designed and tested a MAP processor which relies on this representation and we found it to be more effective than traditional wavelet shrinkage methods both in terms of speckle reduction and signal detail preservation. We evaluated the results on both synthetic data and real SAR images, all coded in eight-bit. Our processor is based on solid statistical theory, and it does not depend on the use of an *ad hoc* thresholding parameter. Hence, the method proposed in Section III-C for choosing the "coring" nonlinearity could be considered as a systematic way of shrinking noisy data, relying on the actual statistics of the signal and noise wavelet coefficients. Naturally, our approach is more computationally expensive due to the fact that the prior distribution parameters need to be estimated at each decomposition scale of interest. However, this is not a serious problem for off-line processing.

It should also be noted that in this work, the parameters of the $S\alpha S$ model are estimated globally within each decomposition scale. For this reason, the shrinking functions shown in Fig. 7 act the same for strong point target and for extended homogenous regions. According to the results, the proposed filter achieves a global compromise between smoothing and edge preservation.

Statistical correlation between adjacent pixels is a result of diffraction effects in the transverse direction and intersymbol interference effects in the range direction [40]. Speckle correlation was not considered in the present work. As we mentioned, this problem can be addressed by image subsampling at the expense of reduced spatial resolution. A more sophisticated approach is to consider the speckle correlation structure into the MAP function. The latter avenue is currently under investigation and results will be reported soon.

Acknowledgment

The authors would like to thank D. E. Wahl (Sandia National Laboratories) for providing part of the SAR imagery used in this research. They are also grateful to J. P. Nolan (American University) who kindly provided his STABLE program in library form.

References

[1] M. Soumekh, *Synthetic Aperture Radar Signal Processing*. New York: Wiley, 1999.

[2] J. W. Goodman, "Some fundamental properties of speckle," *J. Opt. Soc. Amer.*, vol. 66, pp. 1145–1150, Nov. 1976.

[3] V. S. Frost, J. A. Stiles, K. S. Shanmugan, and J. C. Holtzman, "A model for radar images and its application to adaptive digital filtering of multiplicative noise," *IEEE Trans. Pattern Anal. Machine Intell.*, vol. 4, pp. 157–166, 1982.

[4] D. T. Kuan, A. A. Sawchuk, T. C. Strand, and P. Chavel, "Adaptive noise smoothing filter for images with signal-dependent noise," *IEEE Trans. Pattern Anal. Machine Intell.*, vol. 7, pp. 165–177, 1985.
[5] J. S. Lee, "Digital image enhancement and noise filtering by use of local statistics," *IEEE Trans. Pattern Anal. Machine Intell.*, vol. 2, pp. 165–168, 1980.
[6] M. R. Azimi-Sadjadi and S. Bannour, "Two-dimensional adaptive block Kalman filtering of SAR imagery," *IEEE Trans. Geosci. Remote Sensing*, vol. 29, pp. 742–753, 1991.
[7] A. Baraldi and F. Parmigiani, "A refined Gamma MAP SAR speckle filter with improved geometrical adaptivity," *IEEE Trans. on Geosci. and Remote Sensing*, vol. 33, pp. 1245–1257, Sept. 1995.
[8] A. C. Frery, S. J. S. Sant'Anna, N. D. A. Mascarenhas, and O. H. Bustos, "Robust inference techniques for speckle noise reduction in 1-look amplitude SAR images," *Appl. Signal Process.*, vol. 4, pp. 61–76, 1997.
[9] H. Guo, J. E. Odegard, M. Lang, R. A. Gopinath, I. W. Selesnick, and C. S. Burrus, "Wavelet based speckle reduction with application to SAR based ATD/R," in *Proc. 1st Int. Conf. on Image Processing*, vol. 1, Nov. 1994, pp. 75–79.
[10] L. Gagnon and A. Jouan, "Speckle filtering of SAR images—A comparative study between complex-wavelet based and standard filters," *Proc. SPIE*, vol. 3169, pp. 80–91, 1997.
[11] S. Fukuda and H. Hirosawa, "Suppression of speckle in synthetic aperture radar images using wavelet," *Int. J. Remote Sens.*, vol. 19, no. 3, pp. 507–519, 1998.
[12] ——, "Smoothing effect of wavelet-based speckle filtering: The Haar basis case," *IEEE Trans. Geosci. Remote Sensing*, vol. 37, pp. 1168–1172, Mar. 1999.
[13] D. L. Donoho, "Denoising by soft-thresholding," *IEEE Trans. Inform. Theory*, vol. 41, pp. 613–627, May 1995.
[14] E. P. Simoncelli and E. H. Adelson, "Noise removal via Bayesian wavelet coring," in *Proc. 3rd IEEE Int. Conf. on Image Processing*, vol. 1, Sept. 1996, pp. 379–382.
[15] E. P. Simoncelli, "Bayesian denoising of visual images in the wavelet domain," in *Bayesian Inference in Wavelet Based Models*, P. Muller and B. Vidakovic, Eds. New York: Springer-Verlag, June 1999, ch. 18, pp. 291–308.
[16] A. Pizurica, W. Philips, I. Lemahieu, and M. Acheroy, "Despeckling SAR images using wavelets and a new class of adaptive shrinkage estimators," in *Proc. 8th IEEE Int. Conf. on Image Processing*, Oct. 2001, pp. 233–236.
[17] H. Xie, L. E. Pierce, and F. T. Ulaby, "SAR speckle reduction using wavelet denoising and Markov random field modeling," *IEEE Trans. Geosci. Remote Sensing*, vol. 40, pp. 2196–2212, Oct. 2002.
[18] A. Achim, A. Bezerianos, and P. Tsakalides, "Novel Bayesian multiscale method for speckle removal in medical ultrasound images," *IEEE Trans. Med. Imaging*, vol. 20, pp. 772–783, Aug. 2001.
[19] I. A. Koutrouvelis, "Regression-type estimation of the parameters of stable laws," *J. Amer. Statist. Assoc.*, vol. 75, pp. 918–928, Dec. 1980.
[20] S. Cambanis, G. Samorodnitsky, and M. S. Taqqu, Eds., *Stable Processes and Related Topics*. Boston, MA: Birkhauser, 1991.
[21] G. Samorodnitsky and M. S. Taqqu, *Stable Non-Gaussian Random Processes: Stochastic Models With Infinite Variance*. New York: Chapman and Hall, 1994.
[22] C. L. Nikias and M. Shao, *Signal Processing With Alpha-Stable Distributions and Applications*. New York: Wiley, 1995.
[23] R. Adler, R. Feldman, and M. S. Taqqu, *A Guide to Heavy Tails: Statistical Techniques and Applications*. Boston, MA: Birkhauser, 1998.
[24] E. F. Fama and R. Roll, "Some properties of symmetric stable distributions," *J. Amer. Statist. Assoc.*, vol. 63, pp. 817–836, 1968.
[25] W. H. DuMouchel, "Stable distributions in statistical inference," Ph.D. dissertation, Dept. Statist., Yale Univ., New Haven, CT, 1971.
[26] B. W. Brorsen and S. R. Yang, "Maximum likelihood estimates of symmetric stable distribution parameters," *Commun. Statist. Simul.*, vol. 19, pp. 1459–1464, 1990.
[27] J. P. Nolan, "Maximum likelihood estimation and diagnostics for stable distributions," Dept. Math. Statist., American Univ., Tech. Rep., June 1999.
[28] S. Mallat, *A Wavelet Tour of Signal Processing*. New York: Academic, 1998.
[29] S. G. Mallat, "A theory for multiresolution signal decomposition: The wavelet representation," *IEEE Trans. Pattern Anal. Machine Intell.*, vol. 11, pp. 674–692, July 1989.
[30] P. Tsakalides, P. Reveliotis, and C. L. Nikias, "Scalar quantization of heavy-tailed signals," *Proc. Inst. Elect. Eng.*, vol. 147, pp. 475–484, Oct. 2000.
[31] H. H. Arsenault and G. April, "Properties of speckle integrated with a finite aperture and logarithmically transformed," *J. Opt. Soc. Amer.*, vol. 66, pp. 1160–1163, Nov. 1976.
[32] H. Xie, L. E. Pierce, and F. T. Ulaby, "Statistical properties of logarithmically transformed speckle," *IEEE Trans. Geosci. Remote Sensing*, vol. 40, pp. 721–727, Mar. 2002.
[33] C. Oliver and S. Quegan, *Understanding Synthetic Aperture Radar Images*. Norwood, MA: Artech House, 1998.
[34] A. C. Frery, H.-J. Müller, C. C. F. Yanasse, and S. J. S. Sant'Anna, "A model for extremely heterogeneous clutter," *IEEE Trans. Geosci. Remote Sensing*, vol. 35, pp. 648–659, May 1997.
[35] L. M. Kaplan, "Analysis of multiplicative speckle models for template-based SAR ATR," *IEEE Trans. Aerosp. Electron. Syst.*, vol. 37, pp. 1424–1432, Oct. 2001.
[36] I. Daubechies, "Orthonormal bases of compactly supported wavelets," *Commun. Pure Appl. Math.*, vol. 41, pp. 909–996, 1988.
[37] R. R. Coifman and D. L. Donoho, "Translation-invariant de-noising," in *Wavelets and Statistics*, A. Antoniadis, Ed. Berlin, Germany: Springer-Verlag, 1995.
[38] F. Sattar, L. Floreby, G. Salomonsson, and B. Lövström, "Image enhancement based on a nonlinear multiscale method," *IEEE Trans. Image Processing*, vol. 6, pp. 888–895, June 1997.
[39] D. E. Wahl, P. H. Eichel, D. C. Ghiglia, and C. V. Jakowatz, Jr., "Phase gradient autofocus-a robust tool for high resolution SAR phase correction," *IEEE Trans. Aerosp. Electron. Syst.*, vol. 30, pp. 827–835, 1994.
[40] R. N. Czerwinski, D. L. Jones, and W. D. O'Brien, Jr., "Line and boundary detection in speckle images," *IEEE Trans. Image Processing*, vol. 7, pp. 1700–1714, Dec. 1998.

Alin Achim (S'00) was born in Sinaia, Romania, on April 29, 1972. He received the B.S. and M.S. degrees, both in electrical engineering, from Politehnica University of Bucharest, Romania, in 1995 and 1996, respectively, and the Ph.D. degree in biomedical engineering from the University of Patras, Patras, Greece, in 2003.

He is currently a Postdoctoral Fellow with the Department of Medical Physics, University of Patras, Patras, Greece. His research interests include statistical signal processing, multiresolution algorithms, wavelet analysis of medical and radar images, ultrasonic imaging, image filtering and enhancement, and segmentation and classification algorithms. He is coauthor of six journal papers and many conference publications.

Panagiotis Tsakalides (SM'91–M'95) received the Ph.D. degree in electrical engineering from the University of Southern California (USC), Los Angeles, in 1995.

From 1996 to 1998, he was a Research Assistant Professor with the Signal and Image Processing Institute, USC, and he consulted for the U.S. Navy and Air Force. From 1999 to 2002, he was with the Department of Electrical Engineering, University of Patras, Patras, Greece. In September 2002, he joined the Computer Science Department, University of Crete, Heraklion, Greece, as an Associate Professor. His research interests are in the field of statistical signal processing with emphasis in estimation and detection theory, and applications in wireless communications, imaging, and multimedia systems. He has coauthored over 50 technical publications in these areas, including 15 journal papers.

Dr. Tsakalides was awarded the IEE's A. H. Reeve Premium in October 2002 for the paper (coauthored with P. Reveliotis and C. L. Nikias) "Scalar Quantization of Heavy-Tailed Signals," (Oct. 2000, *IEE Proceedings—Vision, Image and Signal Processing*).

Anastasios Bezerianos (M'95) studied physics at Patras University, Patras, Greece, and telecommunications at Athens University, Athens, Greece. He received the Ph.D. degree from Patras Medical School in 1987.

He is an Associate Professor in the Medical School of Patras University and is a Visiting Professor in the Department of Biomedical Engineering, Johns Hopkins University, Baltimore, MD. His research interests are in biomedical signal and image processing and analysis as well as in mathematical models of biological systems. He specializes in nonlinear time series analysis, application of wavelets in signal denoising and pattern recognition, statistical image processing, application of computational intelligence in diagnosis and prognosis of heart diseases and gene expression classification and clustering problems, and one- and two-dimensional heart models. He has in permanent base, cooperation with research centers and university institutes in Japan, the United States, and Europe, and he is reviewer in international scientific journals of the IEEE and IFMBE. His research activities are summarized in three books, 60 scientific publications, and many conference publications.